



Development of multi-component diesel surrogate fuel models – Part II:Validation of the integrated mechanisms in 0-D kinetic and 2-D CFD spray combustion simulations

Poon, Hiew Mun; Pang, Kar Mun; Ng, Hoon Kiat; Gan, Suyin; Schramm, Jesper

Published in:
Fuel

Link to article, DOI:
[10.1016/j.fuel.2016.04.114](https://doi.org/10.1016/j.fuel.2016.04.114)

Publication date:
2016

Document Version
Peer reviewed version

[Link back to DTU Orbit](#)

Citation (APA):

Poon, H. M., Pang, K. M., Ng, H. K., Gan, S., & Schramm, J. (2016). Development of multi-component diesel surrogate fuel models – Part II:Validation of the integrated mechanisms in 0-D kinetic and 2-D CFD spray combustion simulations. *Fuel*, 181, 120-130. <https://doi.org/10.1016/j.fuel.2016.04.114>

General rights

Copyright and moral rights for the publications made accessible in the public portal are retained by the authors and/or other copyright owners and it is a condition of accessing publications that users recognise and abide by the legal requirements associated with these rights.

- Users may download and print one copy of any publication from the public portal for the purpose of private study or research.
- You may not further distribute the material or use it for any profit-making activity or commercial gain
- You may freely distribute the URL identifying the publication in the public portal

If you believe that this document breaches copyright please contact us providing details, and we will remove access to the work immediately and investigate your claim.

1 **Development of Multi-Component Diesel Surrogate Fuel Models - Part II: Validation of**
2 **the Integrated Mechanisms in 0-D Kinetic and 2-D CFD Spray Combustion Simulations**

3 Hiew Mun Poon¹, Kar Mun Pang², Hoon Kiat Ng^{1*}, Suyin Gan³, Jesper Schramm²

4 ¹ *Department of Mechanical, Materials and Manufacturing Engineering, The University of*
5 *Nottingham Malaysia Campus, Jalan Broga, 43500 Semenyih, Selangor, Malaysia.*

6 ² *Department of Mechanical Engineering, Danmarks Tekniske Universitet, Nils Koppels Allé,*
7 *Bygning 403, 2800 Kgs. Lyngby.*

8 ³ *Department of Chemical and Environmental Engineering, The University of Nottingham*
9 *Malaysia Campus, Jalan Broga, 43500 Semenyih, Selangor, Malaysia.*

10 * Corresponding author: Tel: +603 89248161; Fax: +603 89248017; Email-address:
11 hoonkiat.ng@nottingham.edu.my (H.K. Ng)

12 **Abstract**

13 The aim of this study is to develop compact yet comprehensive multi-component diesel
14 surrogate fuel models for computational fluid dynamics (CFD) spray combustion modelling
15 studies. The fuel constituent reduced mechanisms including n-hexadecane (HXN),
16 2,2,4,4,6,8,8-heptamethylnonane (HMN), cyclohexane (CHX) and toluene developed in Part
17 I are applied in this work. They are combined to produce two different versions of multi-
18 component diesel surrogate models in the form of MCDS1 (HXN + HMN) and MCDS2
19 (HXN + HMN + toluene + CHX). The integrated mechanisms are then comprehensively
20 validated in zero-dimensional chemical kinetic simulations under a wide range of shock tube
21 and jet stirred reactor conditions. Subsequently, the fidelity of the surrogate models is further
22 evaluated in two-dimensional CFD spray combustion simulations. Simulation results show
23 that ignition delay (ID) prediction corresponds well to the change of fuel constituent mass
24 fraction which is calculated to match the cetane number (CN). In addition, comparisons of the
25 simulation results to the experimental data of #2 diesel fuel (D2) in a constant volume

26 combustion chamber show that IDs and lift-off lengths are reasonably well replicated by the
27 models. The MCDS2 model is also found to perform better in the soot formation prediction in
28 D2 fuel combustion as the model contains aromatic and cyclo-alkane components which
29 provide an additional pathway to the formation of rich species such as C_2H_2 and C_6H_6 .
30 Implementation of MCDS2 predicts an increase of maximum local soot volume fraction by a
31 factor of 2.1 when the ambient temperature increases from 900K to 1000K, while the
32 prediction by MCDS1 is lower at 1.6. This trend qualitatively agrees with the experimental
33 observation. This work demonstrates that MCDS1 serves as a potential surrogate fuel model
34 for diesel fuels with CN values ranging from 15 to 100. It also shows that MCDS2 is a more
35 appropriate surrogate model for fuels with aromatics and cyclo-paraffinic contents,
36 particularly when soot calculation is of main interest.

37 Keywords: multi-component diesel surrogate, CFD simulations, spray combustion, chemical kinetic
38 mechanism, soot formation.

39 **1. Introduction**

40 In multi-dimensional computational fluid dynamics (CFD) modelling studies [1–6], n-
41 heptane has been widely utilised as a single-component diesel surrogate fuel model owing to
42 its cetane number (CN) of 55, which is comparable to those of the actual diesel fuels which
43 range between 40 to 56 [7]. Nonetheless, actual diesel fuels generally consist of long carbon
44 chain structure with 10 to 25 carbon atoms [7]. Fuels with long-chain n-alkanes exhibit
45 higher reactivity at low temperatures as compared to those with short carbon chains. This is
46 due to the higher ratio of secondary to primary hydrogen atoms which then increases the H-
47 atom abstraction rate during the initiation phase of the oxidation of alkanes [8]. As a
48 consequence, the combustion of long-chain hydrocarbons particularly n-hexadecane (HXN)
49 [9] has become the centre of attention in many current research works [10–13]. HXN is the

50 primary reference fuel and it has a CN of 100. Surrogate fuel models with different CN
51 values can hence be produced when HXN is blended with other fuels such as 1-
52 methyl-naphthalene with a CN of 0 and 2,2,4,4,6,8,8-heptamethylnonane (HMN) with a CN of
53 15. Therefore, HXN has been identified as a promising component for diesel fuel surrogate
54 model in recent works [12–14]. Nonetheless, it is evident that the Hydrogen/Carbon Molar
55 Ratio (H/C) of HXN is different from that of the actual diesel fuels, on top of the difference
56 in CN. H/C ratio is a key property in simulation studies in order to replicate combustion
57 properties such as heat of reaction, local air/fuel stoichiometric location, flame temperature
58 and flame speed [15]. It is important to note that similar restriction is expected to hold for any
59 other single-component diesel surrogate fuels [16,17].

60 Apart from that, the Polycyclic Aromatic Hydrocarbons (PAH) formation in diesel fuel
61 combustion is not well described by a single-component diesel surrogate fuel model [7]. In
62 the experiment carried out by Kook and Pickett [18], soot formation of a surrogate fuel
63 comprising 23% m-xylene and 77% n-dodecane (by volume) was studied and the sooting
64 tendency was subsequently compared to a conventional jet fuel under diesel-engine like
65 conditions. Their planar laser induced incandescence (PLII) measurement revealed that the
66 soot level produced by the n-dodecane/m-xylene surrogate fuel is higher than that of the
67 conventional jet fuel. For the combustion of fuels that do not contain aromatic compounds,
68 the maximum local soot volume fraction (SVF) increases by a factor of approximately two
69 when the ambient temperature rises from 900K to 1000K. On the other hand, the maximum
70 SVF increases by a factor of at least five for the combustion of fuels which consist of
71 aromatic volume of 23% to 27%. This corresponds with the reported experimental studies
72 [19–22] where the sooting tendency of a single-component surrogate model is comparatively
73 less significant than an alkane/aromatic mixture. Single component diesel surrogate models

74 which do not contain PAH chemistry in its original fuel composition are hence debatable
75 since actual diesel fuels contain 20% to 30% of aromatic compounds [23].

76 Recognizing the limitation of single-component diesel surrogate fuel models, development of
77 surrogate models with matching fuel compositions as the actual diesel fuels is necessary.
78 Consequently, multi-component diesel surrogate models with blends of various fuel
79 components have been proposed [7,24–30]. The details of the surrogate mechanisms, together
80 with their respective constitutional components are provided in Table 1. In the earlier years,
81 the number of components in a surrogate model was limited owing to the complexity in
82 solving the stiff ordinary differential equations and the associated high computational cost.
83 Besides, huge quantity of work was required to develop the database and mechanistic
84 understanding of the surrogate components for diesel fuels [7]. Fuel blends which are
85 commonly employed in numerical simulations of diesel combustion are Integrated Diesel
86 European Action (IDEA) mechanism [27,28,31], Primary Reference Fuels (PRF) mechanism
87 [32–35] and Diesel Oil Surrogate (DOS) mechanism [36]. With rapid advancement in
88 chemical kinetics as well as computing power, surrogate models with greater number of fuel
89 components are established such as PRF+1 mechanism [24] and Toluene Reference
90 Fuel/PAH (TRF-PAH) mechanism [25]. Nonetheless, PRF, PRF+1 and TRF-PAH surrogate
91 models are predominantly developed for homogeneous charge compression ignition (HCCI)
92 applications. In these chemical models, n-heptane is mainly employed to represent the n-
93 alkane component. Although the component mass fraction in these fuel blends can be
94 adjusted to generate diesel surrogate models with different CN, the maximum boundary of
95 the CN range is constrained by the CN of n-heptane. Thus, they are not suitable to be used as
96 surrogate models for fuels with higher CN such as a paraffinic diesel reference fuel blend
97 [37] with a CN of 80. More recently, POLIMI_Diesel_201 mechanism has been developed
98 by Ranzi et al. [38] which consists of toluene, xylene, methylnaphthalene and n-alkanes up to

99 HXN. The mechanism was well validated in chemical kinetic simulations through
100 comparison of the ignition delay (ID) predictions with experimental measurements of a
101 binary diesel surrogate mixture under auto-ignition condition [39]. On the other hand, Chang
102 et al. [29] have also formulated a diesel surrogate fuel model comprising toluene, n-decane,
103 iso-octane and methylcyclohexane. These hydrocarbons are selected to represent the
104 aromatics, straight-, branched- and cyclo-alkane components in the actual diesel fuels,
105 respectively. The integrated mechanism was comprehensively validated against the
106 experimental data for each fuel constituent and blends, as well as for practical diesel fuel
107 under wide-ranging operating conditions. However, the performance of these two surrogate
108 models [29,38] is yet to be tested in multi-dimensional CFD modelling studies.

109 Set against this background, this study aims to develop appropriate multi-component diesel
110 surrogate models which account for both diesel fuel ignition and combustion across wider
111 CN range of actual diesel fuels. The reduced models of surrogate components for diesel fuels
112 including HXN, HMN, cyclohexane (CHX) and toluene generated in Part I are applied here.
113 Two combinations of multi-component diesel surrogate models with different fuel
114 compositions and components are developed and first validated in zero-dimensional (0-D)
115 chemical kinetic simulations. The first model consists of straight- and branched-alkanes while
116 the second consists of aromatics, straight-, branched- and cyclo-alkanes. The fidelity of the
117 multi-component models is further appraised through the comparisons made between
118 measurements of a constant volume combustion chamber and the numerical results of two-
119 dimensional (2-D) CFD spray combustion simulations. The study also examines the
120 performance of the surrogate models in predicting soot formation with and without the
121 inclusion of aromatics/cyclo-alkane components.

122 **2. Development and Validations of Multi-Component Diesel Surrogate Fuel Models**

123 In this section, a sequential procedure is applied to formulate the multi-component diesel
124 surrogate models, as illustrated in Fig. 1. The procedure is similar to the model construction
125 scheme of Slavinskaya et al. [40]. Here, a ‘reduced-then-combined’ model construction
126 strategy is employed where the reduced models for each of the fuel components are first
127 derived from the respective detailed models and are subsequently combined together to
128 generate the multi-component diesel surrogate models. As such, the reduced models for each
129 of the components are constructed and may be used for other applications. This strategy also
130 limits errors and complications generated from reducing the combined, detailed surrogate
131 models with more than 3,500 species.

132 The target applications of this work focus on chemical composition match as well as
133 mimicking the combustion and soot precursor formation behaviours of real diesel fuels such
134 as #2 diesel fuel (D2). In this work, the reduced mechanism of HXN is designated as the base
135 mechanism as it is the most abundant and largest hydrocarbon among the fuel constituents.
136 Subsequently, the reduced mechanisms for other surrogate fuel components are added to the
137 base mechanism to generate two combinations of multi-component diesel surrogate models:

- 138 (a) Multi-Component Diesel Surrogate No. 1 (MCDS1): HXN + HMN;
139 (b) Multi-Component Diesel Surrogate No. 2 (MCDS2): HXN + HMN + toluene + CHX.

140 The reduced mechanisms of HXN, HMN and CHX generated in Part I are employed. It is
141 noted that the base chemistries of the fuel constituents are essentially similar as the reactions
142 mechanisms are constructed based on the hierarchical nature of hydrocarbon–oxygen systems
143 [9,41,42] in order to ensure that the results may not be affected when the based model is
144 replaced by different models. The approach is similar to the model construction of the
145 detailed mechanisms of n-heptane and iso-octane by Curran et al. [43,44].

146 The CN of MCDS1 is calculated using Equation (1):

147
$$\text{CN of mixture} = [F_{\text{HXN}} + 0.15F_{\text{HMN}}] \times 100 \quad (1)$$

148 F_{HXN} is the mass fraction of HXN and F_{HMN} is the mass fraction of HMN. The CN and
149 compositions of MCDS1 are determined based on those of Diesel Primary Reference Fuel
150 (DPRF58) [45]. DPRF58 is a fuel mixture of 42% HXN and 58% HMN by mass,
151 corresponding to a CN of 50.7. It was found to yield the same ID timings as the D2 fuel
152 experimentally [46,47]. However, Equation (1) is not applicable for fuel model which
153 considers other components. The compositions of MCDS2 are hence determined based on
154 those of the D2 fuel. The composition of toluene is fixed at 28% which is close to the
155 aromatic composition of D2 provided in the study by Kook and Pickett [48] and it is also
156 approximately the average value of the aromatic composition of typical North American
157 diesel fuels [7]. Subsequently, mass fractions of the remaining fuel components such as
158 HXN, HMN and CHX are iterated to match the IDs of D2. The properties of D2, MCDS1 and
159 MCDS2 surrogate models as well as size of the surrogate models are presented in Table 2.

160 Upon the construction of the multi-component diesel surrogate models, the relative
161 contribution of each reaction pathway to the net production rate of each species has altered as
162 compared with that of the respective single-component model. The reaction pathways of each
163 fuel species in the multi-component diesel surrogate mechanisms are hence reassessed using
164 reaction pathway analysis. It is observed that there are certain species which can be removed
165 from the mechanisms owing to their insignificant effect on the predictions of fuel oxidation
166 process upon integration. One of the examples of the eliminated species is the alkyl radical of
167 HMN, namely HMN-R1. It is formed mainly through H-atom abstraction and alkyl radical
168 decomposition from the fuel species. During the reduction of the detailed HMN mechanism,
169 two isomers of HMN are retained during chain-branching process such as HMN-R8 and
170 HMN-R1. However, when HMN is combined with other fuel components in the MCDS1 and
171 MCDS2 surrogate mechanisms, influence of HMN-R1 onto the formation of intermediate

172 species during chain branching process has become less significant. Therefore, HMN-R1,
173 together with its corresponding reactions and connected species are removed from the
174 mechanism. The species and reaction elimination process is performed in the following steps:

175 (i) Reaction path analysis is carried out for all test conditions. Here, the species for H₂/CO
176 and small hydrocarbon oxidations are not taken into consideration as these pools of
177 species are shared by the fuel constituents in the integrated models. The normalised
178 temperature A-factor sensitivities (as defined in Part I) for all reactions involving the
179 potential eliminable species are calculated. If the sensitivity coefficient values for all the
180 corresponding reactions are lower than the user-specified threshold value (i.e. 0.05)
181 across all the test conditions, the species is then selected for the subsequent elimination
182 procedure.

183 (ii) The model accuracy in ID and species profile predictions is selected as the criterion for
184 the species elimination procedure upon model integration. Hence, the 0-D simulations
185 across all the test conditions are repeated whenever a species is eliminated from the
186 mechanism along with its corresponding elementary reactions so that the model
187 predictions are not affected. The maximum relative error tolerance between the model
188 predictions before and after elimination procedure is retained to within 5%. Sizes of the
189 final, reduced multi-component diesel surrogate models are provided in Table 2.

190 Subsequently, mechanism validations in 0-D simulations are performed using the MCDS1
191 and MCDS2 diesel surrogate models for:

- 192 i) ID timing of each diesel fuel component (Fig. A1 in Appendix A);
- 193 ii) species concentration profiles of each diesel fuel component under auto-ignition (Fig. A2
194 in Appendix A) and JSR conditions (Fig. A3 in Appendix A);
- 195 iii) species concentration profiles of each diesel fuel component in a JSR (Fig. 2); and
- 196 iv) ID timing of DPRF58 [45] and n-dodecane (n-C₁₂H₂₆) [9]. (Fig. 3)

217 The test conditions applied here are described in part I. It is noteworthy that the
218 computational results generated by both multi-component diesel models are plotted together
219 with those predicted by each fuel constituent model. The purpose here is to demonstrate that
220 the performance in predicting the ID timings and species concentrations retains after
221 mechanism integration is carried out.

222 In Fig. A1, the computed IDs for HXN and HMN oxidations using MCDS1 and MCDS2
223 surrogate models are similar as the elementary reactions for HXN and HMN in these two
224 mechanisms are the same. Comparison of ID timings and species profiles with those of CHX
225 detailed mechanism is only performed using MCDS2 as MCDS1 does not contain elementary
226 reactions for CHX. It is observed that the predicted ID timings for each surrogate model
227 agree reasonably well with those of the surrogate components. In addition, trend of the
228 species concentration profiles for both auto-ignition and JSR conditions is retained using both
229 the multi-component surrogate models in comparison with those of each individual diesel
230 fuel component, as shown in Fig. A2 and Fig. A3, respectively. The results for MCDS1 are
231 comparable with those of MCDS2 with only about $\pm 5\%$ deviations. Apart from that, the
232 species concentration profiles in a JSR for each surrogate component are reproduced using
233 the MCDS2 surrogate model. This is demonstrated in Fig. 2. The deviations in the species
234 concentration predictions between the multi-component surrogate models and the individual
235 detailed models for each fuel constituents can be attributed to the influence of kinetic
236 reactions of other fuel components upon model integration. Despite the apparent difference in
237 the absolute values, the relative trends of the species profiles computed by the detailed
238 models are reasonably reproduced by the multi-component surrogate models.

239 Comparisons of the ID timing predictions between the surrogate models and DPRF58 are
240 shown in Fig. 3(a). Agreement is achieved between the multi-component surrogate and
241 DPRF58 mechanisms in ID predictions throughout the test conditions. Largest deviation is

222 observed for initial temperature of 850K and Φ of 1, which is recorded at 33%. The
223 maximum deviations between the computations by the detailed and reduced models are
224 successfully maintained to within an error tolerance of 40%, which is reasonable for large-
225 scale mechanism reduction [51–54]. Apart from that, it is found that MCDS2 with
226 compositions of $F_{\text{HXN}}:F_{\text{HMN}}:F_{\text{C7H8}}:F_{\text{CHX}}$ set to 0.42:0.20:0.28:0.10 yields similar ID timing
227 predictions as DPRF58. In other words, its ignition behaviour is compatible with that of D2.

228 Moreover, the multi-component diesel surrogate mechanisms are further validated in closed
229 homogeneous batch reactor simulations by varying their CN. ID timing predictions are
230 compared in Fig. 3(b) with respect to the detailed n-dodecane mechanism (CN of 87).
231 Composition of $F_{\text{HXN}}:F_{\text{HMN}}$ is set to 0.85:0.15 for MCDS1, corresponding to a CN of 87.25.
232 On the other hand, the fuel composition for MCDS2 is fixed at 0.85:0.15:0:0 for
233 $F_{\text{HXN}}:F_{\text{HMN}}:F_{\text{C7H8}}:F_{\text{CHX}}$. It is observed that the projected ID timings are well replicated using
234 both MCDS1 and MCDS2 diesel surrogate models.

235 Upon the model validations under a series of different test conditions in the 0-D kinetic
236 simulations, the proposed MCDS1 and MCDS2 surrogate models are coupled with CFD
237 models in the next section to simulate spray combustion and soot formation under diesel-
238 engine like conditions.

239 3. 2-D Spray Combustion Simulations

240 In this section, 2-D multi-dimensional CFD simulations are carried out to simulate spray
241 combustion and soot formation processes using both the multi-component diesel surrogate
242 fuel models. The spray combustion solver in OpenFOAM-2.0.x is used and a multistep soot
243 model is integrated into the solver [55]. The numerical setups for the reacting diesel fuel
244 sprays are described in Table 3(a). Further description of the numerical setups can be found
245 in the former work [12,13]. In this work, the physical properties of the aromatic compounds

246 are represented by those of toluene. On the other hand, the physical properties of the alkanes
247 are represented by the physical properties of n-tetradecane as its physical properties are close
248 to those of real diesel fuels. Thus, the influence of fuel physical properties is isolated and the
249 effect of the chemical kinetics of reaction models can be studied.

250 Based on the sensitivity study shown in [56], the spatial and temporal evolutions of fourth
251 aromatic ring PAH, pyrene, are similar to those of smaller PAHs or C_2H_2 when the flame
252 temperature is relatively high (typically under no or low EGR conditions). Hence,
253 implementation of C_2H_2 as soot precursor is usually a good compromise between results
254 accuracy and simplicity when the PAH chemistry is absent [4,57–59]. C_2H_2 is selected as the
255 soot precursor in the numerical simulations using the MCDS1 surrogate model as this
256 mechanism does not contain PAH mechanism. On the other hand, C_6H_6 is present in the
257 MCDS2 surrogate model when CHX mechanism is integrated into the multi-component
258 mechanism during the model development stage. With the presence of the PAH chemistry in
259 the surrogate model, C_6H_6 is therefore designated as the soot precursor species in the
260 respective modelling studies. In order to simulate the mass addition on soot particle surface,
261 C_2H_2 is consistently used as the soot surface growth species when MCDS1 and MCDS2 are
262 applied. On the other hand, OH and O_2 are set as the soot oxidant species for the calculation
263 of soot mass destruction.

264 In this section, the numerical simulations are separated into two parts. First and foremost,
265 MCDS1 is applied in a sensitivity test to examine its reactivity towards variation in CN. Mass
266 fractions of HXN and HMN as well as the corresponding CN are shown in Table 3(b). It is
267 then followed by the validation of both MCDS1 and MCDS2 using the measurements of D2
268 fuel [18,48] from constant volume combustion chamber experiments. Mass fraction of each
269 component is varied to mimic the actual fuel properties, which are detailed in Table 2.
270 Operating conditions used for this validation exercise are demonstrated in Table 3(c).

271 Measurements are available for reacting spray test cases at 15% O₂ mole fraction. This
272 condition represents a reactive environment of air diluted with exhaust gas recirculation. The
273 ambient temperature varies from 900K to 1000K while the ambient density is fixed at
274 22.8kg/m³. The computed ID, lift-off length (LOL) and SVF are compared to the
275 experimental data. For the simulation results, ID is defined as the maximum dT/dt gradient of
276 the temperature profile. On the other hand, LOL is defined as the distance from the injector to
277 the closest layer where OH mass fraction reaches 2% of its maximum value in the domain.
278 These definitions correspond with those recommended by Engine Combustion Network [50].

279 *3.1 Sensitivity Test of the MCDS1 Surrogate Model on CN Variations*

280 The effects of variation in CN on LOL and ID predictions are demonstrated in Fig. 4(a). As
281 the CN increases, it is expected that the ID becomes shorter. Thus, the ignition occurs at a
282 location closer to the injection tip and the associated flame lift-off is hence shorter. The trend
283 is replicated by the model. Based on the results shown in Fig. 4(a), it is observed that the
284 kinetics of MCDS1 surrogate model is sensitive to changes in CN ranging from 15 to 100.
285 MCDS1 serves as a promising surrogate model for diesel fuels with various CN.

286 In the next section, the MCDS1 model is further validated using the D2 fuel data. Its
287 performance is also compared against that of the counterpart MCDS2 which considers CHX
288 and toluene reactions.

289 *3.2 Validation using D2 experimental data*

290 The predicted IDs and LOLs by MCDS1 and MCDS2 surrogate models for D2 fuel
291 combustion at ambient temperatures of 900K and 1000K are demonstrated in Fig. 4(b). It is
292 observed that the predictions follow the overall trend where the calculated ID and LOL
293 decrease with increasing ambient temperature. The maximum deviations in ID and LOL

294 predictions with respect to the experimental measurements retain within 15.4% and 23%,
295 respectively. The IDs calculated using MCDS1 agree well with the measurements in both
296 cases but shorter LOLs are produced. On the other hand, the predicted IDs and LOLs are
297 slightly longer in both cases when MCDS2 is applied. This can be attributed to the inclusion
298 of toluene which is difficult to ignite. As it is considered in the initial composition of the
299 MCDS2 model, the resulting ID becomes longer. The flame hence stabilises at a location
300 further downstream from the injection tip, yielding a longer LOL. It is noted that the
301 deviations between the experimental and computed LOLs using MCDS2 are less pronounced,
302 where deviations of 3.5mm and 2.5mm are recorded for ambient temperatures of 900K and
303 1000K, respectively. It is worth mentioning that the deviations between the measured and
304 computed LOLs can also be attributed to the absence of turbulence – chemistry interaction
305 (TCI) in the numerical computations. Inclusion of TCI effects has been shown important to
306 improve the prediction of the OH distributions and hence the development of flame lift-off
307 [60–62].

308 In addition, the SVF predictions of D2 fuel using MCDS1 and MCDS2 are demonstrated in
309 Fig. 5(a). The predictions are compared with the experimental soot clouds [18] obtained at
310 quasi-steady state (4ms after start of injection) for ambient temperatures of 900K and 1000K.
311 These experimental soot images are obtained from the PLII measurement which provides
312 two-dimensional information of SVF distributions for D2 fuel. The red dashed lines on the
313 images indicate the flame LOLs and only qualitative information of soot distribution in the
314 fuel jets is provided based on the images obtained from the experiment. In Fig. 5(a), it is
315 observed that the soot length predicted by MCDS2 is similar to that of the experimental
316 measurements for D2 fuel combustion at ambient temperatures of 900K and 1000K. In
317 contrast, the simulated soot clouds appear to be larger than the soot clouds observed in the
318 experiments for both cases when MCDS1 is employed. In comparison to the predictions of

319 MCDS2, the soot clouds predicted by MCDS1 are formed at further upstream locations closer
320 to the injection tip. This can be attributed to the associated shorter LOLs. Subsequently,
321 quantitative SVF predictions along spray axis at quasi-steady state for D2 fuel combustion
322 are demonstrated in Fig. 5(b). Results in Fig. 5(b) shows that the local SVF values produced
323 by MCDS1 and MCDS2 are different. MCDS1 estimates maximum local SVF values of
324 15ppm and 24ppm for the 900K and 1000K test cases, respectively. On the other hand, the
325 maximum local SVF values predicted by MCDS2 for the 900K and 1000K test cases are
326 5.8ppm and 12.2ppm, respectively. It is observed that the local SVF given by MCDS1 is
327 consistently higher than that of MCDS2. This can be attributed to several reasons. First of all,
328 the LOLs predicted by MCDS1 are shorter. The associated amount of air entrained into the
329 fuel rich core region is lesser. Besides this, MCDS1 utilises C_2H_2 as soot precursor while
330 MCDS2 uses C_6H_6 . The mass concentration of C_2H_2 is commonly higher than that of PAH,
331 leading to higher level of soot inception rate and hence soot mass gained. Lastly, as compared
332 to MCDS1, the amount of branched-alkane (i.e. HMN) used in the initial fuel composition of
333 the MCDS2 model is lower. As a consequence, the production rate of C_2H_2 drops and the
334 soot mass gained through the soot surface growth process decreases correspondingly,
335 yielding lower SVF values.

336 The next parameter used to evaluate the performance of the multi-component surrogate
337 models is the soot formation behaviour at different ambient temperatures. The results
338 indicates that the predicted maximum local SVF increases by a factor of 1.6 as the ambient
339 temperature is raised from 900K to 1000K when MCDS1 is applied. The use of MCDS2
340 increases the maximum local SVF by a factor of 2.1. The ratio of increment in maximum
341 SVF from ambient temperature of 900K to 1000K is henceforth represented by $ratio_{SVF}$ for
342 brevity. Based on the measurement presented by Kook and Pickett [18], the experimental
343 $ratio_{SVF}$ is more than three for D2 fuel combustion. The use of MCDS2 is found to improve

344 the overall simulated ratio_{SVF}. This can be attributed to the inclusion of aromatic and cyclo-
345 alkane components in the initial fuel composition in MCDS2. At different ambient
346 temperatures, the production of C₂H₂ is different when the aromatic and cyclo-alkane
347 components are considered and omitted. This is further elaborated in the subsequent section.

348 Numerical analysis of C₂H₂ and C₆H₆ formations is performed at times when temperature
349 rises by 100K, 200K, 400K, 800K and 1000K from the initial ambient temperatures. The
350 results are demonstrated in Fig. 6 and the temperature tolerance for this comparison study is
351 ± 20 K. Besides these, C₂H₂ and C₆H₆ formations at quasi-steady state are also provided, in
352 which the computed results are obtained at 4ms after the time of injection to ensure that the
353 formation of the selected species in all test cases reaches a quasi-steady state. The
354 observations obtained from the numerical analysis are discussed below:

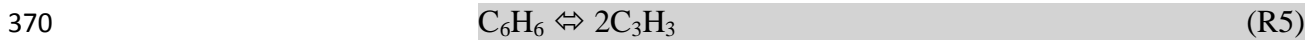
355 (i) Results in Fig. 6(a) depict that the amount of C₂H₂ produced at the temperature rise of
356 100K from the initial ambient temperatures of 900K and 1000K is lower than C₆H₆ when
357 both MCDS1 and MCDS2 are applied. C₆H₆ is mainly produced through the breakdowns
358 of cyclo-paraffin ring as well as toluene via R1 to R4.



363 (ii) At temperature interval of 200K from the initial ambient temperatures, it is observed that
364 the maximum values of C₂H₂ calculated using MCDS2 are approximately two-fold and
365 five-fold greater than those predicted by MCDS1 in the 900K and 1000K cases,
366 respectively. This is depicted in Fig. 6(b). The apparent differences in the predicted C₂H₂
367 levels can be attributed to the significant amount of C₆H₆ produced by MCDS2, which

368 subsequently leads to higher production rate of C_2H_2 as compared to that of MCDS1.

369 The key formation pathways to C_2H_2 from C_6H_6 are described by reactions R5 to R7.



373 (iii) In Fig. 6(c), it is observed that the peak mass fractions of C_2H_2 in the 1000K cases are

374 consistently higher than those in the 900K cases when the initial ambient temperatures

375 increase by 400K, disregards the use of MCDS1 and MCDS2. This is due to the higher

376 production rate of C_2H_2 from the dissociation of C_6H_6 by R5 to R7 using MCDS2 as well

377 as the consumption of C_2H_4 using both MCDS1 and MCDS2 in the 1000K cases. The

378 formation of C_2H_2 is significantly dependent on C_2H_4 and the main formation pathways

379 from C_2H_4 to C_2H_2 are described by reactions R8 to R10.



383 (iv) At temperature interval of 800K from the initial ambient temperatures, the associated

384 mass fractions of C_2H_2 predicted by MCDS1 start to grow significantly and the peak

385 values match with those produced by MCDS2, as demonstrated in Fig. 6(d). As

386 discussed in the previous section, MCDS1 contains higher amount of branched-alkane in

387 the initial fuel composition. As a result, the production rate of C_2H_2 becomes higher than

388 that of MCDS2 which eventually results in the current observation.

389 (v) Same observation as of Fig. 6(d) persists until approaching ignition points.

390 (vi) The associated mass fractions of C_2H_2 continue to rise and eventually those predicted by

391 MCDS1 become higher for both 900K and 1000K cases upon reaching a quasi-steady

392 state, as illustrated in Fig. 6(f). This corresponds well with the earlier findings in Fig.
393 5(b), in which SVF predictions by MCDS2 are lower for both 900K and 1000K cases.

394 The current results suggest that the MCDS1 model is useful for the soot formation
395 simulations where the effect of aromatic chemistry plays a less significant role. For instance,
396 Vishwanathan and Reitz [63] reasonably captured the variation of SVF with respect to the
397 change of injection pressure and injector diameter using a single-component surrogate model,
398 namely n-heptane, showing that the presence of aromatic compounds has less pronounced
399 impact on such application. On the other hand, this work demonstrates that the overall soot
400 formation predictions have been improved by considering cyclo-alkane and aromatic
401 compounds. The revised counterpart, MCDS2, is found to predict a higher $\text{ratio}_{\text{SVF}}$ when the
402 ambient temperature varies. Yet, the computed $\text{ratio}_{\text{SVF}}$ is under-predicted as compared to that
403 of the experiment measurement where $\text{ratio}_{\text{SVF}} > 3$ is recorded. Further improvement is
404 necessary on the coupled MCDS2-soot model to simulate the complex soot formation
405 phenomenon.

406 The ambient pressure is increased to retain the ambient density of 22.8kg/m^3 as the ambient
407 temperature varies between 900K and 1000K in the current test cases. However, the
408 conventional multistep soot model does not capture pressure effects of soot formation [56].
409 The current soot model assumes that soot particles grow primarily by the addition of gaseous
410 C_2H_2 . The use of a pressure dependent surface growth model constant is expected to improve
411 $\text{ratio}_{\text{SVF}}$. Alternatively, the inclusion of PAH condensation effects on soot formation under
412 such high pressure, high temperature environment may aid to improve the prediction as well.
413 Bisetti et al. [64] who implemented Hybrid Method of Moments in their Direct Numerical
414 Simulation of soot formation in the n-heptane/air turbulent non-premixed flame revealed that
415 PAH condensation is significant to the soot mass generation.

416 It is noteworthy that NO_x submodel was not included in the multi-component diesel
417 surrogate fuel models. Despite of this, these fuel models are expected to produce reasonable
418 predictions for thermal NO_x, which is the major portion of NO_x emissions in conventional
419 diesel engines. Thermal NO_x formation rate is highly dependent on temperature [65], hence
420 reasonable predictions of the temperature is the pre-requisite for the associated calculation.
421 In the current numerical simulations, the maximum local temperatures calculated by the
422 integrated fuel models are between 2300K and 2400K. These predictions are consistent with
423 those obtained in the study of Pickett et al. [66] for 15% ambient oxygen. Apart from these, it
424 is noteworthy that the accurate predictions of OH concentrations are essential for simulating
425 thermal NO_x formation. Based on the kinetic studies in the 0-D simulations (as shown in Fig.
426 A2 and A3 in Appendix A), it is observed that the OH mole fractions predicted by the
427 integrated models correspond reasonably well with the computations of the detailed models.
428 However, it should also be highlighted that the computation of thermal NO_x emissions also
429 depends on the associated Arrhenius rate constants [67]. Hence, the surrogate models can be
430 useful for thermal NO_x simulations only when they are integrated with the extended
431 Zeldovich reaction rates which are validated for engine applications.

432 4. Conclusions

433 In this study, two multi-component diesel surrogate models namely MCDS1 and MCDS2
434 with different fuel compositions and components have been introduced. MCDS1 model
435 consists of straight- (HXN) and branched- (HMN) alkanes while MCDS2 consists of
436 aromatic hydrocarbon (toluene), straight- (HXN), branched- (HMN) and cyclo- (CHX)
437 alkanes. Surrogate fuel models with CN values ranging from 15 to 100 can be produced
438 through blending of HXN and HMN. In addition, CHX and toluene are incorporated into
439 MCDS2 model to achieve compositional match and to improve soot formation predictions.
440 The integrated models are comprehensively validated in 0-D chemical kinetic simulations

441 under a wide range of shock tube and JSR conditions, by comparing the computations to
442 those predicted by each detailed and reduced fuel constituent models. It is found that
443 performance of the surrogate models in ID and species concentration predictions under both
444 auto-ignition and JSR conditions is maintained after mechanism integration. Apart from
445 these, the integrated models are also validated against the JSR experimental results for each
446 diesel fuel constituents. Overall agreement between the computations and measurements is
447 achieved with maximum deviations of one order of magnitude on the absolute values.
448 Following that, the fidelity of both multi-component diesel surrogate models is further
449 assessed in the 2-D spray combustion simulations. Numerical results reveal that MCDS1 is
450 sensitive to the change of CN. The predicted ID and LOL correspond well with the variation
451 of CN. Next, ID, LOL and SVF calculated using MCDS1 and MCDS2 are validated against
452 constant volume combustion chamber experimental data. ID and LOL predictions given by
453 both surrogate models agree reasonably well with the D2 measurements. Besides, it is
454 observed that MCDS2 is able to provide better predictions in soot formation events than
455 MCDS1 due to the inclusion of aromatic and cyclo-alkane components. It is revealed that
456 $\text{ratio}_{\text{SVF}}$ of 1.6 is obtained for D2 fuel combustion when the ambient temperature increases
457 from 900K to 1000K with the absence of aromatic and cyclo-alkane components. The
458 simulated $\text{ratio}_{\text{SVF}}$ increases to 2.1 when both components are incorporated into the base
459 mechanism as the inclusion of these two components provides alternative pathways to form
460 rich species such as C_2H_2 and C_6H_6 . In this work, the effects of including aromatic and cyclo-
461 alkane components in the surrogate model on soot formation events are highlighted. It is
462 demonstrated that MCDS2 is a potential surrogate model for D2 fuel. Nonetheless, additional
463 work is required to improve the coupled MCDS2-soot model in simulating the complex soot
464 formation phenomenon.

465 **Acknowledgements**

466 The Ministry of Higher Education Malaysia is acknowledged for the financial support
467 towards this project under the Fundamental Research Grant Scheme (FRGS) F0014.54.02.
468 The work at Technical University of Denmark is supported by Innovation Fund Denmark and
469 MAN Diesel & Turbo A/S through the RADIADe project.

470 **References**

- 471 [1] Som S, Aggarwal SK. Effects of Primary Breakup Modeling on Spray and Combustion
472 Characteristics of Compression Ignition Engines. *Combust Flame* 2010;157:1179–93.
- 473 [2] Ma G, Tauzia X, Maiboom A. One-Dimensional Combustion Model with Detailed
474 Chemistry for Transient Diesel Sprays. *Proc Inst Mech Eng Part D: J Automob Eng*
475 2014;228:457–76.
- 476 [3] Pang KM, Ng HK, Gan S. In-Cylinder Diesel Spray Combustion Simulations Using
477 Parallel Computation: A Performance Benchmarking Study. *Appl Energy*
478 2012;93:466–78.
- 479 [4] Bolla M, Wright YM, Boulouchos K, Borghesi G, Mastorakos E. Soot Formation
480 Modeling of n-Heptane Sprays Under Diesel Engine Conditions Using the Conditional
481 Moment Closure Approach. *Combust Sci Technol* 2013;185:766–93.
- 482 [5] Pitsch H, Wan YP, Peters N. Numerical Investigation of Soot Formation and
483 Oxidation Under Diesel Engine Conditions. SAE Tech Paper 952357; 1995.
- 484 [6] Singh S, Reitz RD, Musculus MPB. Comparison of the Characteristic Time (CTC),
485 Representative Interactive Flamelet (RIF), and Direct Integration with Detailed
486 Chemistry Combustion Models against Optical Diagnostic Data for Multi-Mode
487 Combustion in a Heavy-Duty DI Diesel Engine. SAE Technical Paper 2006-01-0055;
488 2006.
- 489 [7] Farrell JT, Cernansky NP, Dryer FL, Law CK, Friend DG, Hergart CA, et al.
490 Development of an Experimental Database and Kinetic Models for Surrogate Diesel
491 Fuels. SAE Technical Paper 2007-01-0201; 2007.
- 492 [8] Sahetchian KA, Blin N, Rigny R, Seydi A, Murat M. The Oxidation of n-Butane and
493 n-Heptane in a CFR Engine. Isomerization Reactions and Delay of Autoignition.
494 *Combust Flame* 1990;79:242–9.
- 495 [9] Westbrook CK, Pitz WJ, Herbinet O, Curran HJ, Silke EJ. A Comprehensive Detailed
496 Chemical Kinetic Reaction Mechanism for Combustion of n-Alkane Hydrocarbons
497 from n-Octane to n-Hexadecane. *Combust Flame* 2009;156:181–99.
- 498 [10] Naik CV, Puduppakkam K, Meeks E, Liang L. Ignition Quality Tester Guided
499 Improvements to Reaction Mechanisms for n-Alkanes: n-Heptane to n-Hexadecane.
500 SAE Technical Paper 2012-01-0149; 2012.
- 501 [11] Ristori A, Dagaut P, Cathonnet M. The Oxidation of n-Hexadecane: Experimental and
502 Detailed Kinetic Modeling. *Combust Flame* 2001;125:1128–37.
- 503 [12] Poon HM, Ng HK, Gan S, Pang KM, Schramm J. Evaluation and Development of
504 Chemical Kinetic Mechanism Reduction Scheme for Biodiesel and Diesel Fuel
505 Surrogates. *SAE Int J Fuels Lubr* 2013;6:729–44.
- 506 [13] Poon HM, Ng HK, Gan S, Pang KM, Schramm J. Development and Validation of
507 Chemical Kinetic Mechanism Reduction Scheme for Large-Scale Mechanisms. *SAE*
508 *Int J Fuels Lubr* 2014;7:653–62.
- 509 [14] Cowart JS, Fischer WP, Hamilton LJ, Caton PA, Sarathy SM, Pitz WJ. An
510 Experimental and Modeling Study Investigating the Ignition Delay in a Military Diesel

- 511 Engine Running Hexadecane (Cetane) Fuel. *Int J Engine Res* 2012;14:57–67.
- 512 [15] Dryer FL, Ju Y, Brezinsky K, Santoro RJ, Litzinger TA, Sung C-J. Science-Based
513 Design of Fuel-Flexible Chemical Propulsion/Energy: Generation of Comprehensive
514 Surrogate Kinetic Models and Validation Databases for Simulating Large Molecular
515 Weight Hydrocarbon Fuels. AF Office of Scientific Research Final Report, Grant No.
516 FA9550-07-1-0515; 2012.
- 517 [16] Meijer M. Characterization of n-Heptane as a Single Component Diesel Surrogate
518 Fuel. Technical University of Eindhoven Automotive Technology, Graduation Thesis;
519 2010.
- 520 [17] Galle J, Sebastian V. Influence of Diesel Surrogates on the Behavior of Simplified
521 Spray Models. *Proc FISITA 2012 World Automot Congr* 2013;189:361–74.
- 522 [18] Kook S, Pickett LM. Soot Volume Fraction and Morphology of Conventional, Fischer-
523 Tropsch, Coal-Derived, and Surrogate Fuel at Diesel Conditions. *SAE Int J Fuels Lubr*
524 2012;5:647–64.
- 525 [19] Lemaire R, Faccinetto A, Therssen E, Ziskind M, Focsa C, Desgroux P. Experimental
526 Comparison of Soot Formation in Turbulent Flames of Diesel and Surrogate Diesel
527 Fuels. *Proc Combust Inst* 2009;32 I:737–44.
- 528 [20] Barths H, Pitsch H, Peters N. 3D Simulation of DI Diesel Combustion and Pollutant
529 Formation Using a Two-Component Reference Fuel. *Oil Gas Sci Technol*
530 1999;54:233–44.
- 531 [21] Dagaut P, Cathonnet M. The Ignition, Oxidation, and Combustion of Kerosene: A
532 Review of Experimental and Kinetic Modeling. *Prog Energy Combust Sci*
533 2006;32:48–92.
- 534 [22] Mathieu O, Djebaili-Chaumeix N, Paillard CE, Douce F. Experimental Study of Soot
535 Formation from a Diesel Fuel Surrogate in a Shock Tube. *Combust Flame*
536 2009;156:1576–86.
- 537 [23] Pitz WJ, Mueller CJ. Recent Progress in the Development of Diesel Surrogate Fuels.
538 *Prog Energy Combust Sci* 2011;37:330–50.
- 539 [24] Chaos M, Zhao Z, Kazakov A, Gokulakrishnan P, Angioletti M, Dryer FL. A PRF +
540 Toluene Surrogate Fuel Model for Simulating Gasoline Kinetics. In: 5th US Combust
541 Meet 2007:1–19.
- 542 [25] Wang H, Jiao Q, Yao M, Yang B, Qiu L, Reitz RD. Development of an n-
543 Heptane/Toluene/Polyaromatic Hydrocarbon Mechanism and Its Application for
544 Combustion and Soot Prediction. *Int J Engine Res* 2013;14:434–51.
- 545 [26] Westbrook CK, Pitz WJ, Mehl M, Curran HJ. Detailed Chemical Kinetic Reaction
546 Mechanisms for Primary Reference Fuels for Diesel Cetane Number and Spark-
547 Ignition Octane Number. *Proc Combust Inst* 2011;33:185–92.
- 548 [27] Schindler K. Integrated Diesel European Action (IDEA): Study of Diesel
549 Combustion. SAE Technical Paper 920591; 1992.
- 550 [28] Hentschel W, Schindler K, Haahtela O. European Diesel Research IDEA-Experimental
551 Results from DI Diesel Engine Investigations. SAE Technical Paper 941954; 1994.
- 552 [29] Chang Y, Jia M, Li Y, Liu Y, Xie M, Wang H, et al. Development of a Skeletal
553 Mechanism for Diesel Surrogate Fuel by Using a Decoupling Methodology. *Combust*
554 *Flame* 2015;162:3785–802.
- 555 [30] Frassoldati A, D’Errico G, Lucchini T, Stagni A, Cuoci A, Faravelli T, et al. Reduced
556 Kinetic Mechanisms of Diesel Fuel Surrogate for Engine CFD Simulations. *Combust*
557 *Flame* 2015;162:3991–4007.
- 558 [31] Hergart C, Barths H, Peters N. Modeling the Combustion in a Small-Bore Diesel
559 Engine Using a Method Based on Representative Interactive Flamelets. SAE Technical
560 Paper 1999-01-3550; 1999.

- 561 [32] Curran H, Pitz W, Westbrook C, Callahan CV, Dryer FL. Oxidation of Automotive
562 Primary Reference Fuels at Elevated Pressures. *Proc Combust Inst* 1998;27:379–87.
- 563 [33] Kirchen P, Shahbakhti M, Koch CR. A Skeletal Kinetic Mechanism for PRF
564 Combustion in HCCI Engines. *Combust Sci Technol* 2007;179:1059–83.
- 565 [34] Wang H, Yao M, Reitz RD. Development of a Reduced Primary Reference Fuel
566 Mechanism for Internal Combustion Engine Combustion Simulations. *Energy & Fuels*
567 2013;27:7843–53.
- 568 [35] Lawrence Livermore National Laboratory Physical and Life Sciences Directorate.
569 Available from: [https://combustion.llnl.gov/archived-mechanisms/surrogates/prf-](https://combustion.llnl.gov/archived-mechanisms/surrogates/prf-isooctane-n-heptane-mixture)
570 [isooctane-n-heptane-mixture](https://combustion.llnl.gov/archived-mechanisms/surrogates/prf-isooctane-n-heptane-mixture).
- 571 [36] Golovitchev VI, Bergman M, Montorsi L. CFD Modeling of Diesel Oil and DME
572 Performance in a Two-Stroke Free Piston Engine. *Combust Sci Technol*
573 2007;179:417–36.
- 574 [37] Pickett LM, Siebers DL. Fuel Effects on Soot Processes of Fuel Jets at DI Diesel
575 Conditions. *SAE Technical Paper* 2003-01-3080; 2003.
- 576 [38] Ranzi E, Frassoldati A, Stagni A, Pelucchi M, Cuoci A, Faravelli T. Reduced Kinetic
577 Schemes of Complex Reaction Systems: Fossil and Biomass-Derived Transportation
578 Fuels. *Int J Chem Kinet* 2014;46:512–42.
- 579 [39] Wang H, Warner SJ, Oehlschlaeger MA, Bounaceur R, Biet J, Glaude PA, et al. An
580 Experimental and Kinetic Modeling Study of the Autoignition of α -
581 Methyl-naphthalene/Air and α -Methyl-naphthalene/n-Decane/Air Mixtures at Elevated
582 Pressures. *Combust Flame* 2010;157:1976–88.
- 583 [40] Slavinskaya N, Zizin A, Riedel U. Towards Kerosene Reaction Model Development:
584 Propylcyclohexane, C_9H_{18} , n-Dodecane, $\text{C}_{12}\text{H}_{26}$, and Hexadecane $\text{C}_{16}\text{H}_{34}$
585 combustion. *AIAA* 2010:1–13.
- 586 [41] Oehlschlaeger MA, Steinberg J, Westbrook CK, Pitz WJ. The Autoignition of iso-
587 Cetane at High to Moderate Temperatures and Elevated Pressures: Shock Tube
588 Experiments and Kinetic Modeling. *Combust Flame* 2009;156:2165–72.
- 589 [42] Silke EJ, Pitz WJ, Westbrook CK, Ribaucour M. Detailed Chemical Kinetic Modeling
590 of Cyclohexane Oxidation. *J Phys Chem A* 2007;111:3761–75.
- 591 [43] Curran HJ, Gaffuri P, Pitz WJ, Westbrook CK. A Comprehensive Modeling Study of
592 n-Heptane Oxidation. *Combust Flame* 1998;114:149–77.
- 593 [44] Curran HJ, Gaffuri P, Pitz WJ, Westbrook CK. A comprehensive Modeling Study of
594 iso-Octane Oxidation. *Combust Flame* 2002;129:253–80.
- 595 [45] Perini F, Sahoo D, Miles P, Reitz R. Modeling the Ignitability of a Pilot Injection for a
596 Diesel Primary Reference Fuel: Impact of Injection Pressure, Ambient Temperature
597 and Injected Mass. *SAE Int J Fuels Lubr* 2014:48–64.
- 598 [46] Sahoo D, Petersen B, Miles P. Measurement of Equivalence Ratio in a Light-Duty
599 Low Temperature Combustion Diesel Engine by Planar Laser Induced Fluorescence of
600 a Fuel Tracer. *SAE Int J Engines* 2011;4:2312–25.
- 601 [47] Petersen B, Miles PC, Sahoo D. Equivalence Ratio Distributions in a Light-Duty
602 Diesel Engine Operating Under Partially Premixed Conditions. *SAE Int J Engines*
603 2012;5:526–37.
- 604 [48] Kook S, Pickett LM. Liquid Length and Vapor Penetration of Conventional, Fischer–
605 Tropesch, Coal-Derived, and Surrogate Fuel Sprays at High-Temperature and High-
606 Pressure Ambient Conditions. *Fuel* 2012;93:539–48.
- 607 [49] Yaws CL. *Thermophysical Properties of Chemicals and Hydrocarbons*. Elsevier; 2009.
- 608 [50] Engine Combustion Network Experimental Data Archive. Available from:
609 <http://www.sandia.gov/ecn/>.
- 610 [51] Brakora JL, Ra Y, Reitz RD. Combustion Model for Biodiesel-Fueled Engine

- 611 Simulations Using Realistic Chemistry and Physical Properties. SAE Int J Engines
612 2011;4:931–47.
- 613 [52] Niemeyer KE, Sung C-J, Raju MP. Skeletal Mechanism Generation for Surrogate
614 Fuels Using Directed Relation Graph with Error Propagation and Sensitivity Analysis.
615 Combust Flame 2010;157:1760–70.
- 616 [53] Yang J, Johansson M, Naik C, Puduppakkam K, Golovitchev V, Meeks E. 3D CFD
617 Modeling of a Biodiesel-Fueled Diesel Engine Based on a Detailed Chemical
618 Mechanism. SAE Technical Paper 2012-01-0151; 2012.
- 619 [54] Luo Z, Plomer M, Lu T, Som S, Longman DE, Sarathy SM, et al. A Reduced
620 Mechanism for Biodiesel Surrogates for Compression Ignition Engine Applications.
621 Fuel 2012;99:143–53.
- 622 [55] Leung KM, Lindstedt RP, Jones WP. A Simplified Reaction Mechanism for Soot
623 Formation in Nonpremixed Flames. Combust Flame 1991;87:289–305.
- 624 [56] Pang KM, Jangi M, Bai X-S, Schramm J. Evaluation and Optimisation of
625 Phenomenological Multi-Step Soot Model for Spray Combustion Under Diesel
626 Engine-Like Operating Conditions. Combust Theory Model 2015:1–30.
- 627 [57] Jangi M, Lucchini T, D’Errico G, Bai X-S. Effects of EGR on the Structure and
628 Emissions of Diesel Combustion. Proc Combust Inst 2013;34:3091–8.
- 629 [58] Pang KM, Jangi M, Bai X-S, Schramm J. Investigation of Chemical Kinetics on Soot
630 Formation Event of n-Heptane Spray Combustion. SAE Technical Paper 2014-01-
631 1254; 2014.
- 632 [59] Kong S-C, Sun Y, Rietz RD. Modeling Diesel Spray Flame Liftoff, Sooting Tendency,
633 and NO_x Emissions Using Detailed Chemistry with Phenomenological Soot
634 Model. J Eng Gas Turbines Power 2007;129:245–51.
- 635 [60] D’Errico G, Lucchini T, Contino F, Jangi M, Bai X-S. Comparison of Well-Mixed and
636 Multiple Representative Interactive Flamelet Approaches for Diesel Spray Combustion
637 Modelling. Combust Theory Model 2014;18:65–88.
- 638 [61] Bhattacharjee S, Haworth DC. Simulations of Transient n-Heptane and n-Dodecane
639 Spray Flames Under Engine-Relevant Conditions Using a Transported PDF Method.
640 Combust Flame 2013;160:2083–102.
- 641 [62] Pei Y, Hawkes ER, Kook S. A Comprehensive Study of Effects of Mixing and
642 Chemical Kinetic Models on Predictions of n-Heptane Jet Ignitions with the PDF
643 Method. Flow, Turbul Combust 2013;91:249–80.
- 644 [63] Vishwanathan G, Reitz RD. Development of a Practical Soot Modeling Approach and
645 Its Application to Low-Temperature Diesel Combustion. Combust Sci Technol
646 2010;182:1050–82.
- 647 [64] Bisetti F, Blanquart G, Mueller ME, Pitsch H. On the Formation and Early Evolution
648 of Soot in Turbulent Nonpremixed Flames. Combust Flame 2012;159:317–35.
- 649 [65] Christensen M, Hultqvist A, Johansson B. Demonstrating the Multi Fuel Capability of
650 a Homogeneous Charge Compression Ignition Engine with Variable Compression
651 Ratio. SAE Technical Paper 1999-01-3679; 1999.
- 652 [66] Pickett L, Siebers D, Idicheria C. Relationship Between Ignition Processes and the
653 Lift-Off Length of Diesel Fuel Jets. SAE Technical Paper 2005-01-3843; 2005.
- 654 [67] Hernández JJ, Pérez-Collado J, Sanz-Argent J. Role of the Chemical Kinetics on
655 Modeling NO_x Emissions in Diesel Engines. Energy & Fuels 2008;22:262–72.
- 656

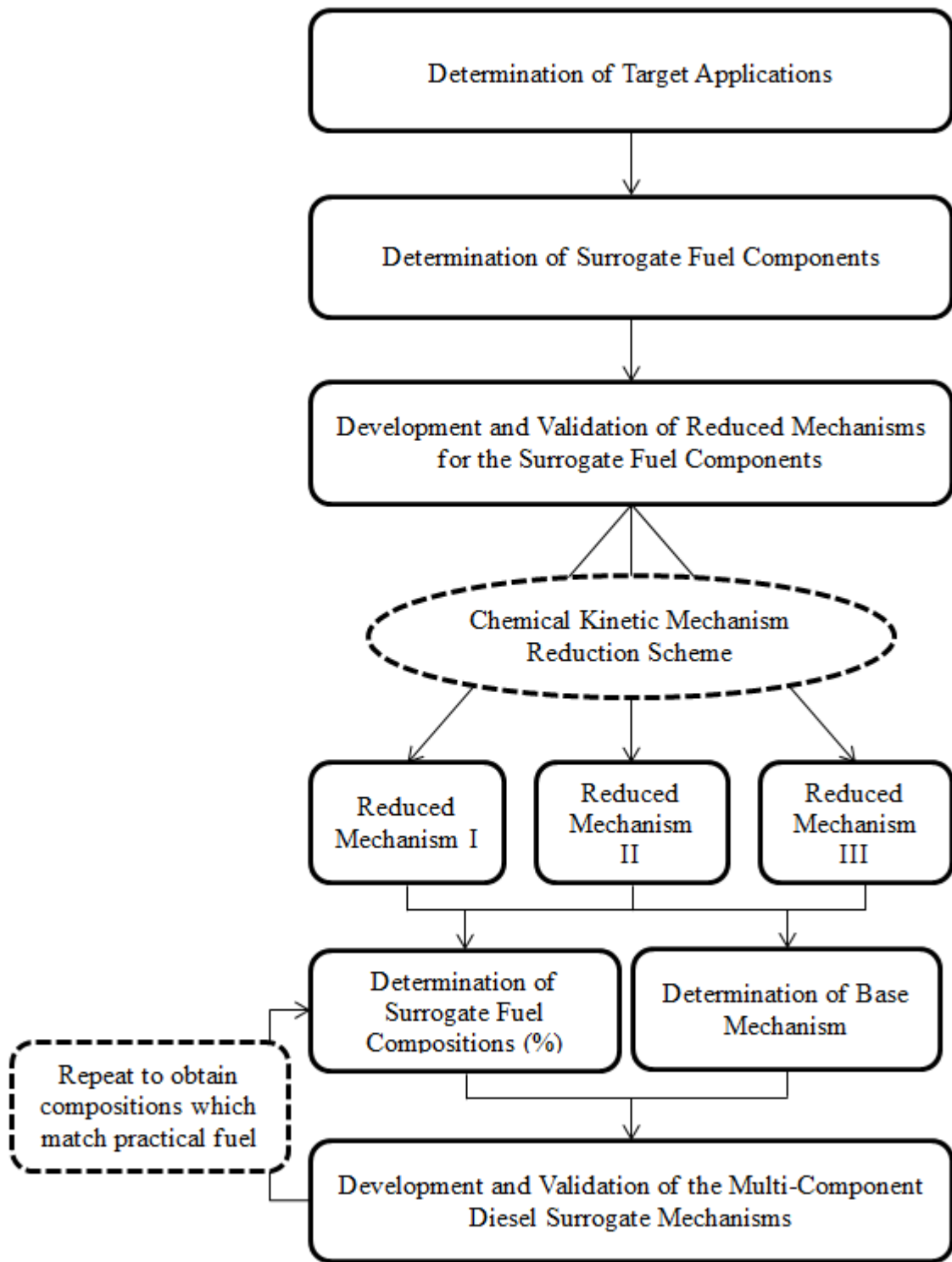


Fig. 1 Sequential steps to formulate the multi-component diesel surrogate fuel models.

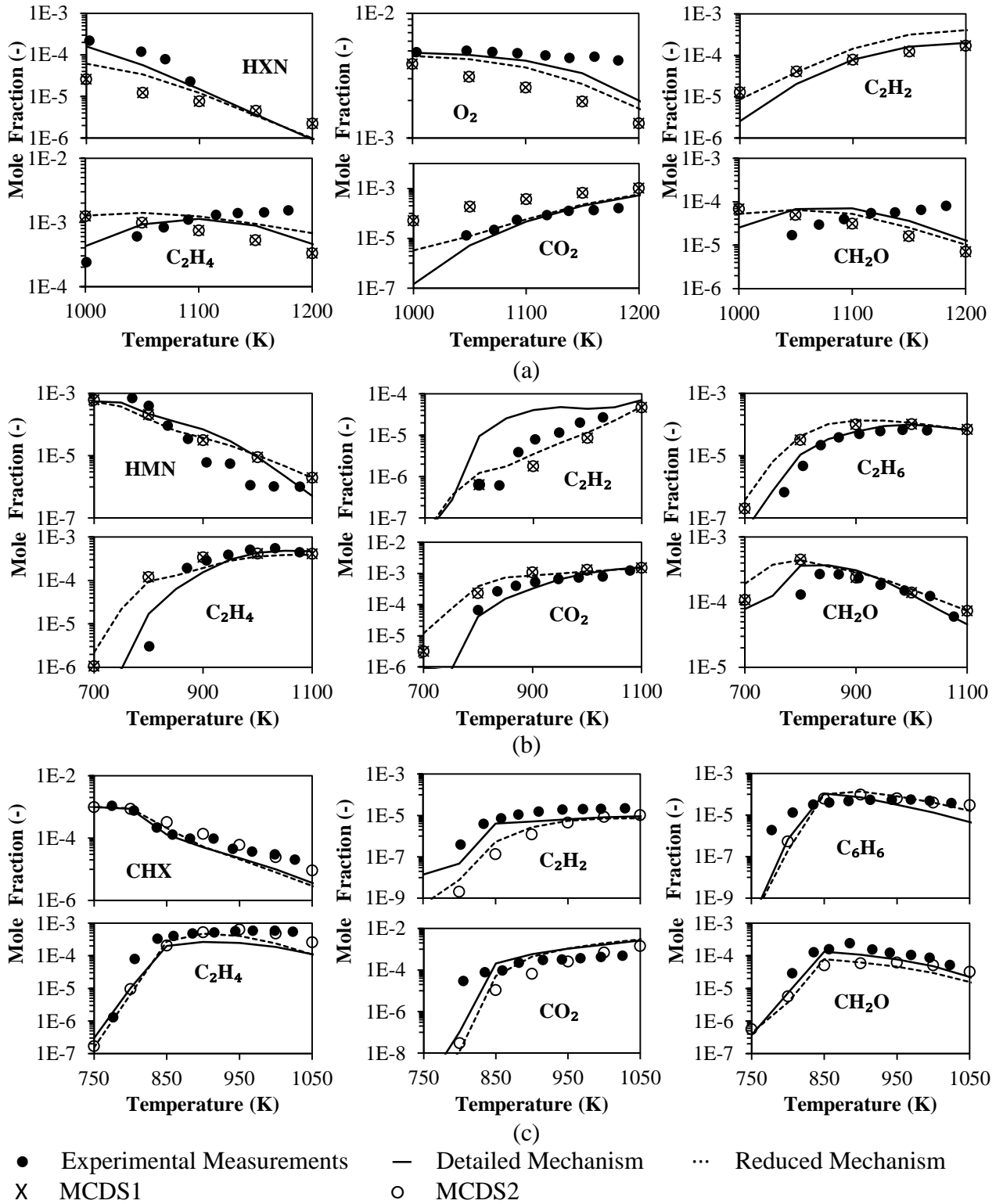


Fig. 2 Computed and experimental species mole fractions obtained from the oxidation of (a) 0.03% HXN (pressure = 1atm, $\Phi = 1.5$, residence time = 70ms), (b) 0.07% HMN (pressure = 10atm, $\Phi = 2$, residence time = 1s), and (c) 0.1% CHX (pressure = 10atm, $\Phi = 1.5$, residence time = 0.5s) under JSR conditions.

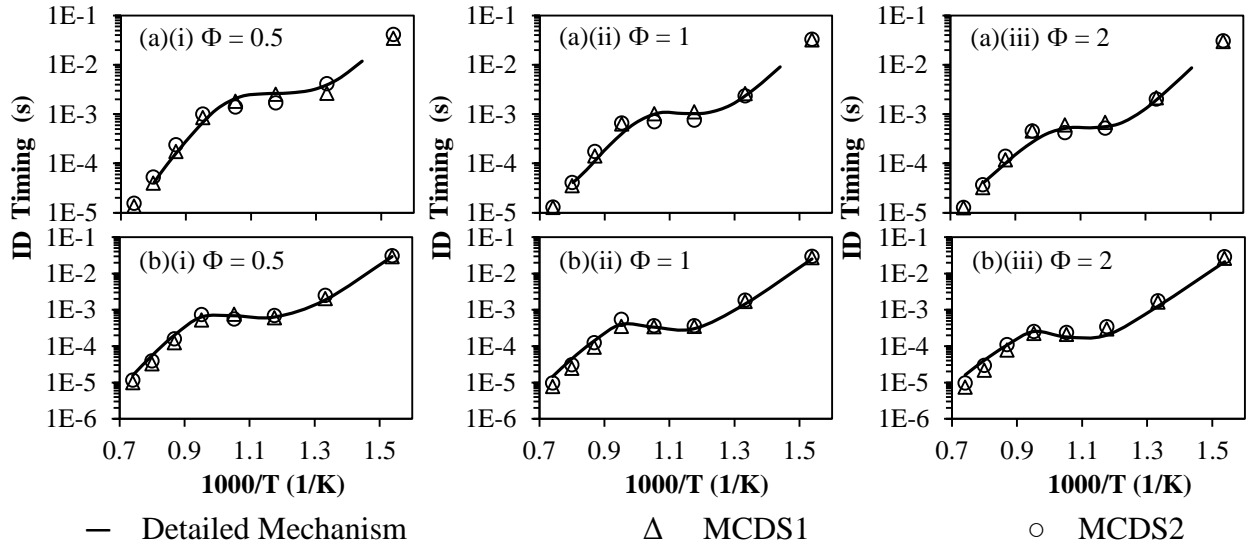


Fig. 3 Comparisons of the ID predicted by MCDS1 and MCDS2 surrogate models with the detailed mechanisms of (a) DPRF58^a [45] and (b) n-dodecane^b [9] for initial pressure of 40bar, Φ of (i) 0.5, (ii) 1 and (iii) 2. [^aID_s of DPRF58 were computed by Perini et al. [45] using the detailed mechanism of Westbrook et al. [26] in a constant volume vessel using identical initial conditions; ^bThe mechanism of n-dodecane was extracted from the detailed mechanism of Westbrook et al. [9] for combustion of n-alkane hydrocarbons from n-octane to HXN.]

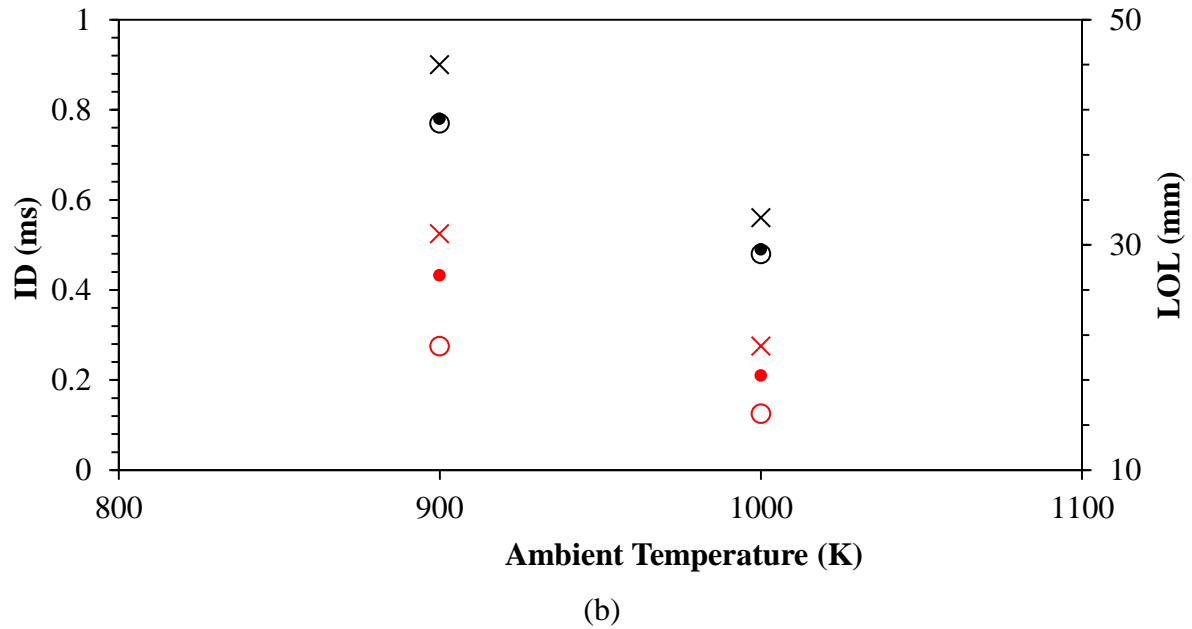
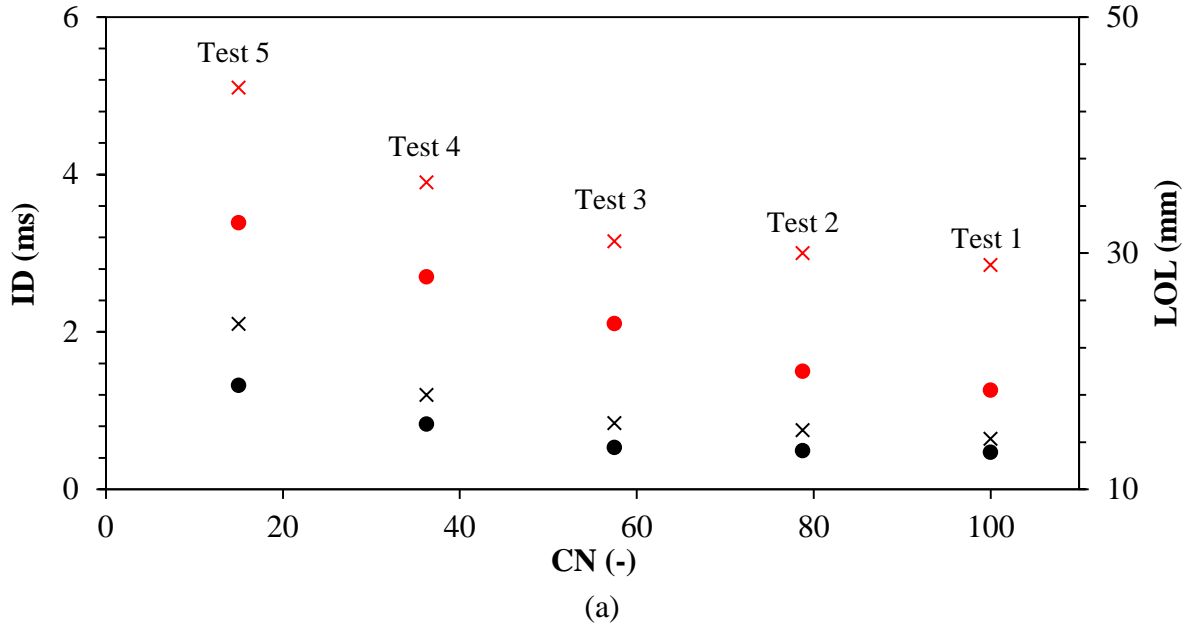


Fig. 4 (a) ID (black) and LOL (red) predictions against CN for the sensitivity tests using MCDS1 surrogate model for ambient temperatures of 900K (x) and 1000K (●); (b) ID (black) and LOL (red) predictions using MCDS1 (○) and MCDS2 (x) surrogate models in comparison with the experimental measurements (●) for D2 fuel combustion for ambient temperatures of 900K and 1000K.

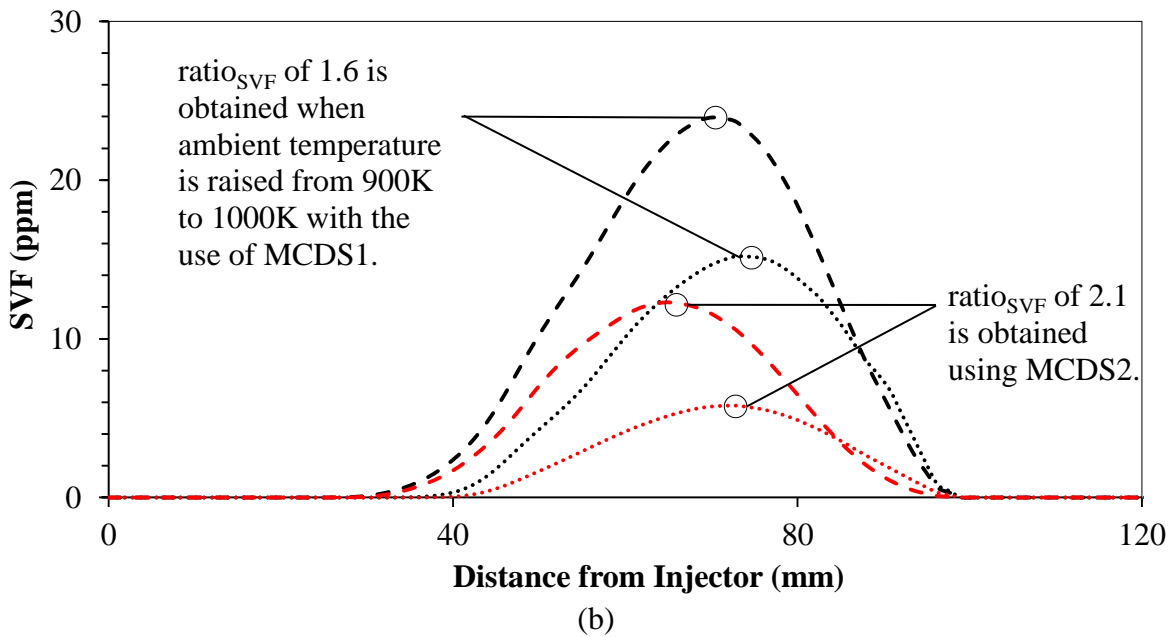
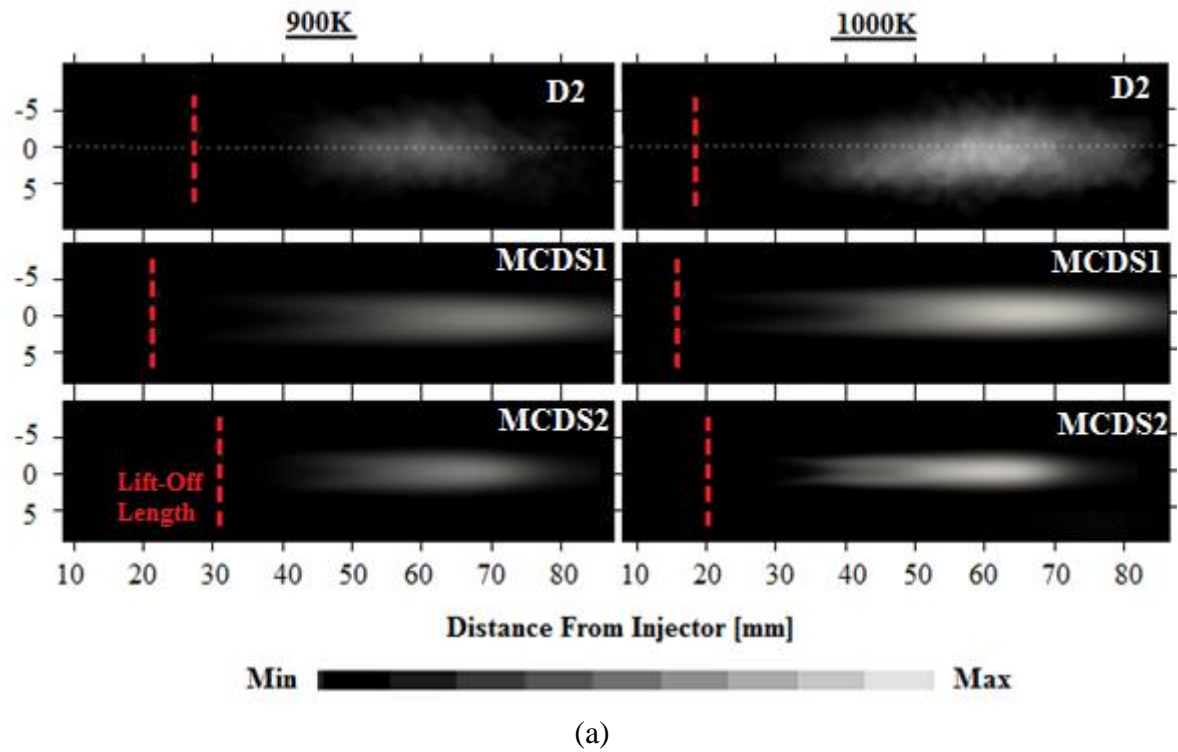


Fig. 5 (a) Qualitative comparisons of predicted SVF contours and experimental soot cloud images at quasi-steady state for D2 fuel combustion in a constant volume chamber using MCDS1 and MCDS2 surrogate models; (b) Comparisons of the computed SVF along spray axis using MCDS1 (black) and MCDS2 (red) surrogate models at ambient temperatures of 900K (···) and 1000K (---).

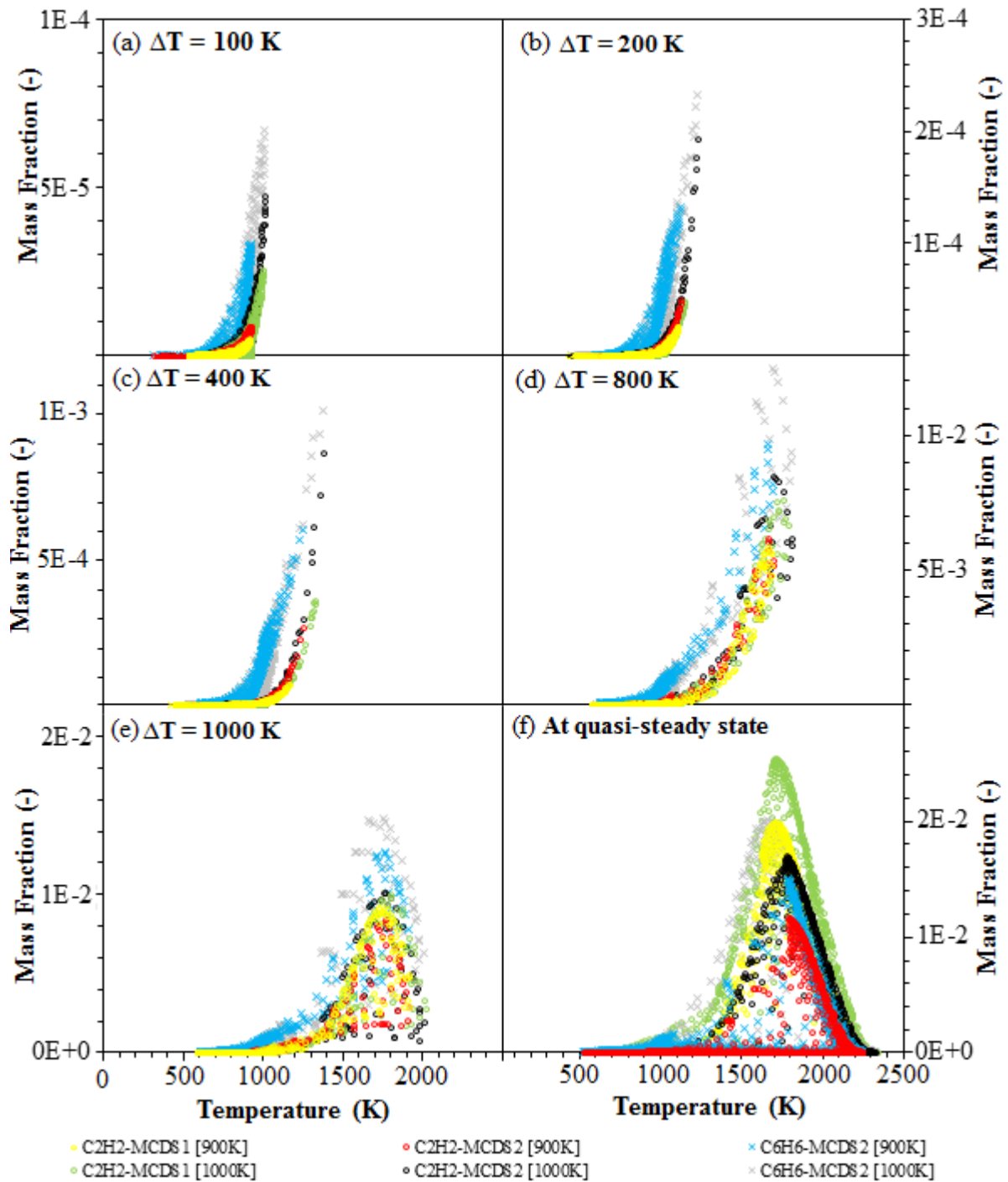


Fig. 6 Comparisons of C_2H_2 and C_6H_6 mass fractions at temperature intervals of (a) 100K, (b) 200K, (c) 400K, (d) 800K, (e) 1000K and at (f) quasi-steady state for D2 fuel combustion at ambient temperatures of 900K and 1000K using MCDS1 and MCDS2 diesel surrogate models. [Note: Mass fractions of C_6H_6 at $\Delta T = 100K$, $\Delta T = 200K$ and $\Delta T = 400K$ are scaled down by a factor of 20, 10 and 5, respectively.]**

Table 1 Details of the currently available multi-component surrogate fuel models.

Surrogate Models	Compositions	N_S	N_R	Model Descriptions	Year of Publication	Author(s)	Ref.
IDEA	n-decane, 1-methylnaphthalene	118	557	Describe fuel oxidation, soot and NO _x formations; Contain low-temperature kinetics for auto-ignition.	1999	Hergart et al.	[31]
PRF	iso-octane, n-heptane	990	4,060	Describe auto-ignition and intermediate product formation at high-pressure conditions; Contain kinetic reactions for low to high temperatures as well as NTC behaviour.	1998	Curran et al.	[32]
		58	120	Describe ignition of PRF in a HCCI engine; Contain kinetic reactions for intermediate and high temperatures.	2007	Kirchen et al.	[33]
		73	296	Describe oxidation of diesel/gasoline; Contain kinetic reactions for low to high temperatures as well as NTC behaviour. Reduced model of Wang et al. [34] is developed based on the LLNL detailed model [35].	2013	Wang et al.	[34]
		1,034	4,236		-	LLNL	[35]
Diesel PRF	HXN, HMN	2,800	11,000	Contain alkylperoxy radical sub-mechanism and kinetic reactions for low to high temperatures as well as NTC behaviour.	2011	Westbrook et al.	[26]
DOS	n-heptane, toluene	70	305	Describe fuel oxidation, soot and NO _x formations; Optimised for engine applications.	2007	Golovitchev et al.	[36]
PRF+1	iso-octane, n-heptane, toluene	469	1,221	Describe fuel oxidation and soot formations; Contain kinetic reactions for low and intermediate temperatures.	2007	Chaos et al.	[24]
TRF-PAH	n-heptane, toluene, PAH	71	360	Describe combustion and PAH formation; Contain kinetic reactions for low to high temperatures.	2013	Wang et al.	[25]
POLIMI_Diesel_201	HXN, toluene, xylene, methylnaphthalene	201	4,240	Validated under shock-tube (intermediate to high temperatures) and JSR (low to intermediate temperatures) simulations.	2014	Ranzi et al.	[38]
POLIMI_NC12_96 + PAH	n-dodecane, PAH	133	2,275	Contain kinetic reactions for low to high temperatures; Reasonably capture the important characteristics of spray ignition processes.	2015	Frassoldati et al.	[30]
Skeletal Diesel Surrogate Fuel Model	n-decane, iso-octane, methylcyclohexane, toluene	70	220	Validated under shock-tube, JSR, flow reactor and pre-mixed laminar flame simulations.	2015	Chang et al.	[29]

N_S and N_R denote the number of species and reactions, respectively; NTC is defined as negative temperature coefficient.

Table 2 Fuel properties [18,48-50] and chemistry sizes of detailed/reduced chemical mechanism models used in the current work.

Properties	D2	MCDS1	MCDS2
Chemical Formula (mass fraction)	C ₃ -C ₂₅	F _{HXN} : F _{HMN} = 0.42 : 0.58	F _{HXN} : F _{HMN} : F _{toluene} : F _{CHX} = 0.42 : 0.20 : 0.28 : 0.10
Type of Hydrocarbon	33.8% ^a / 27% ^b Aromatics, 65.0% ^a Alkanes, 1.2% ^a Olefins	Straight- and branched-alkanes	Straight-, branched- and cyclo-alkanes, aromatic
CN	46 (40-56)	50.7	-
Molecular Weight [g/mol]	~200.000	226.446	174.612
H/C Ratio	1.800	2.125	1.838
Lower Heating Value [MJ/kg]	42.975	43.900 ^c	42.928 ^c
Boiling Point [°C]	350	287	287
Flash Point [°C]	73.0	111.5 ^c	74.7 ^c
Size of final reduced mechanism (<i>N_S</i> ; <i>N_R</i>)	-	128; 408 ^d 88; 284 ^e	169; 545 ^d 129; 411 ^e

F denotes mass fraction

^aComposition of aromatic compounds provided in the study of Pickett and Siebers [37]

^bComposition of aromatic compounds provided in the study of Kook and Pickett [48]

^cVolume-averaged properties are given for MCDS1 and MCDS2

^dBefore elimination of unimportant species and reactions upon integration

^eAfter elimination of unimportant species and reactions upon integration

Table 3 (a) CFD model setups used for reacting diesel fuel spray simulations; (b) Sensitivity test with various CN using MCDS1 surrogate model; (c) Experimental operating conditions.

(a) Numerical Setups		
Grid	Grading; 0.25mm x 0.25mm (minimum), 4mm x 2mm (maximum) in both radial and axial directions	
Turbulence Model	Standard k - ϵ ($C_\mu = 0.09$; $C_1 = 1.54$; $C_2 = 1.92$; $C_3 = -0.33$; $\sigma_k = 1$; $\sigma_\epsilon = 1.3$)	
Breakup Model	Reitz Diwakar ($C_{bag} = 6$; $C_b = 0.785$; $C_{strip} = 0.5$; $C_s = 12$)	
Soot Model	Multi-step [55]	
Time Step (s)	5.00E-07	
Number of Parcels	100,000	
Initial k (m^2/s^2)	0.735	
Initial ϵ (m^2/s^3)	3.5	
(b) Sensitivity Test with Various CN		
Tests	Compositions ($F_{H2N}:F_{HMN}$)	CN
1	1:0	100
2	0.75:0.25	78.75
3	0.50:0.50	57.5
4	0.25:0.75	36.25
5	0:1	15
(c) Experimental Operating Conditions		
Ambient temperature (K)	900/1000	
Ambient density (kg/m^3)	22.8	
Ambient Pressure (MPa)	6/6.7	
Orifice diameter (mm)	0.09	
Ambient composition (%)	$O_2 = 15\%$; $CO_2 = 6.23\%$; $H_2O = 3.62\%$; $N_2 = 75.15\%$	
Injection duration (ms)	7	

k and ϵ denote the turbulence kinetic energy and turbulence dissipation rate, respectively

Appendix A: Validation Results for 0-D Chemical Kinetic Simulations

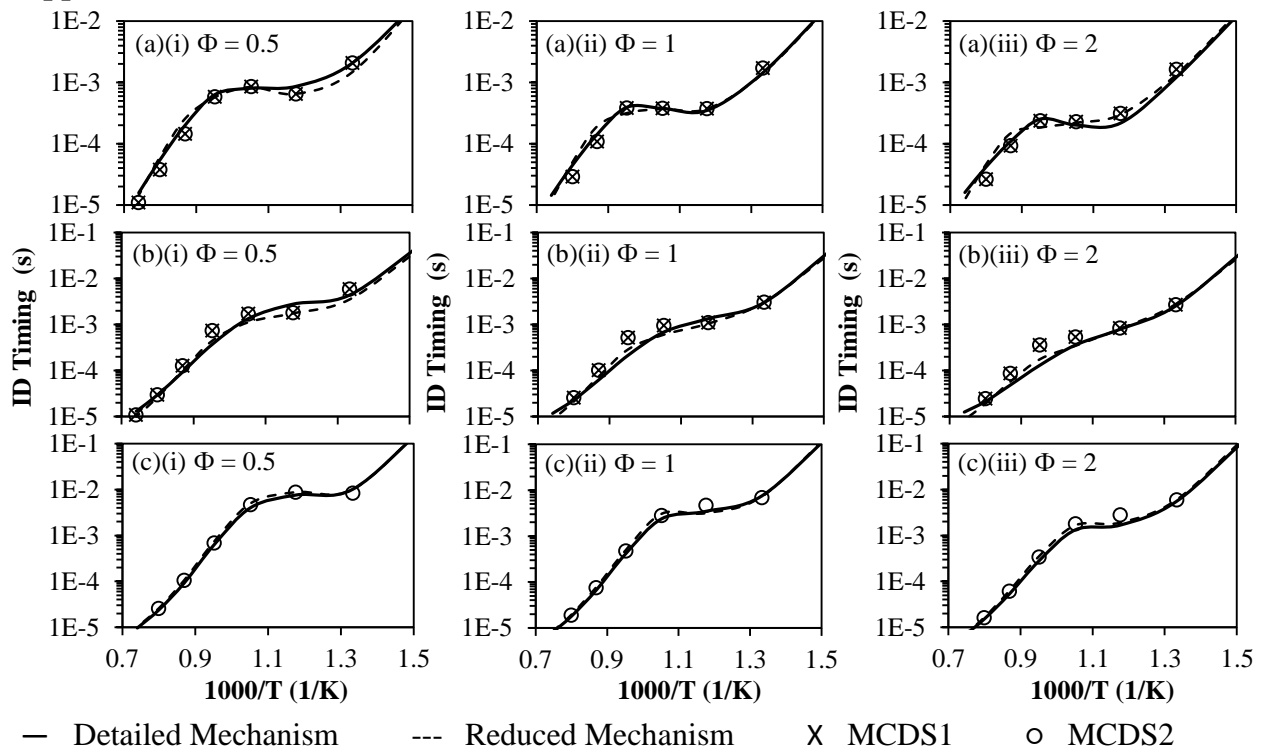


Fig. A1 Computed ID of (a) HXN, (b) HMN and (c) CHX calculated by respective detailed and reduced mechanisms as well as MCDS1 and MCDS2 surrogate models, with initial pressure of 60bar and Φ of (i) 0.5, (ii) 1.0, (iii) 2.0.

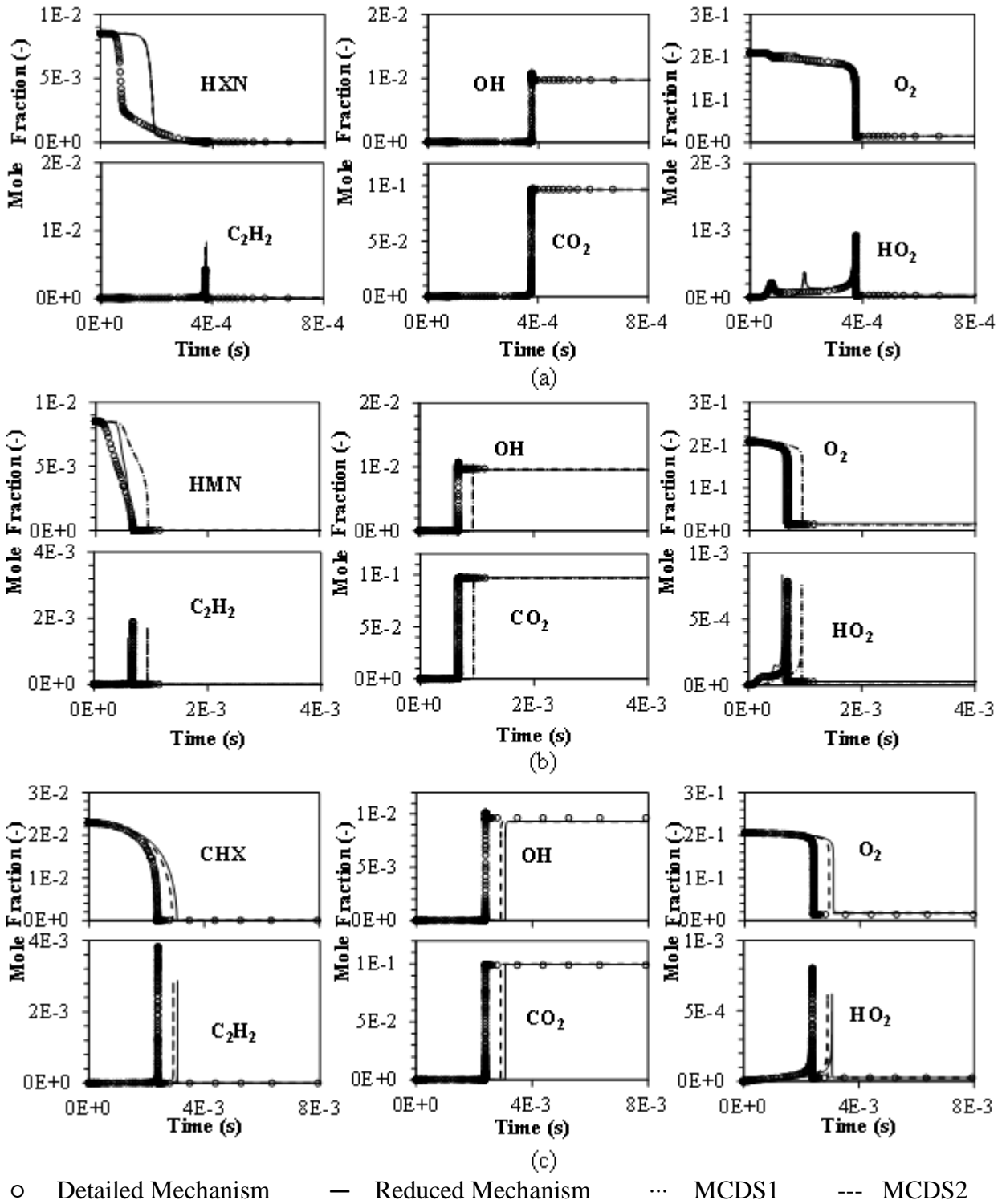


Fig. A2 Computed species profiles for (a) HXN, (b) HMN and (c) CHX combustions under auto-ignition condition, with initial pressure of 60bar, initial temperature of 950K and Φ of 1.

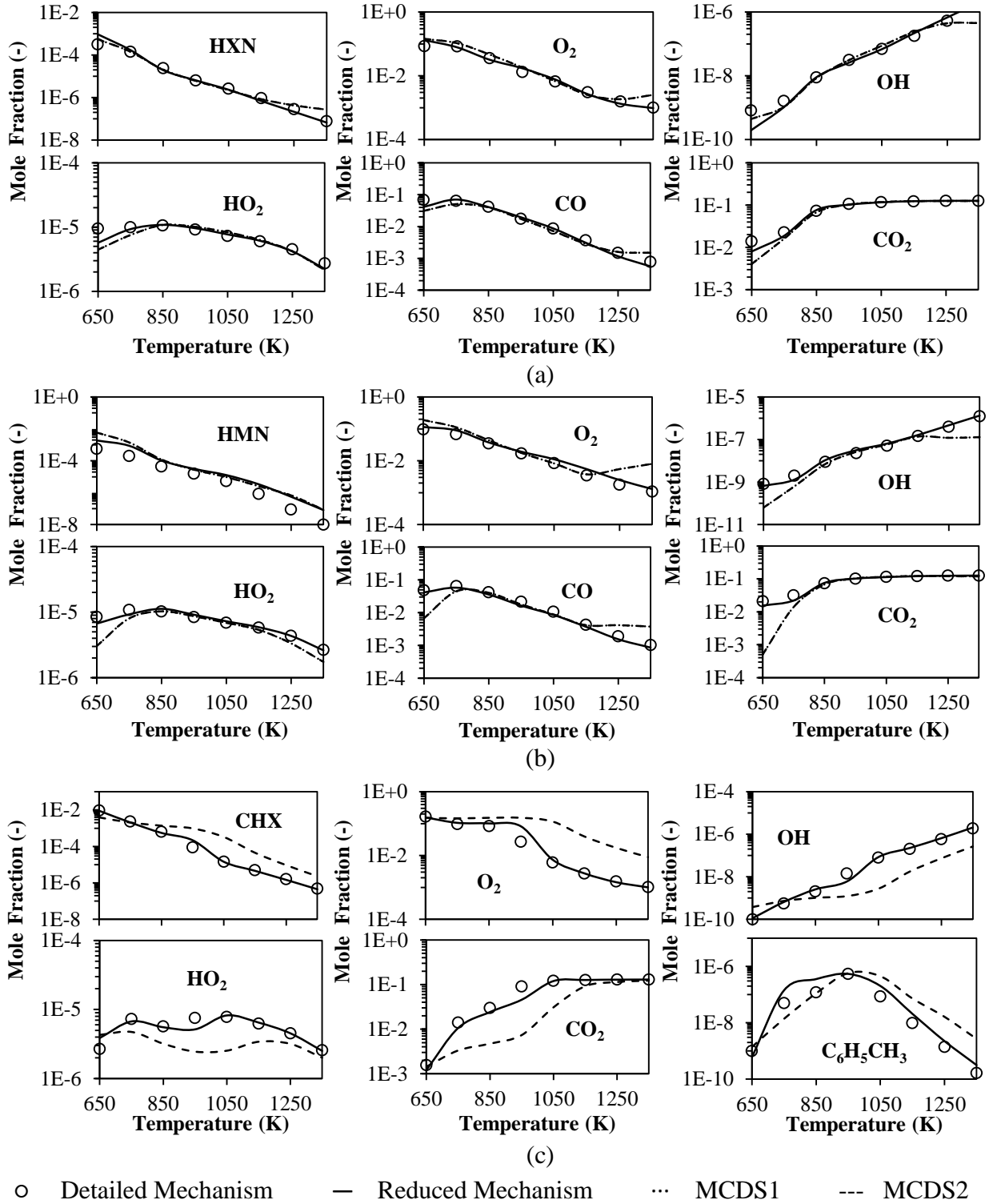


Fig. A3 Computed species profiles of (a) HXN, (b) HMN and (c) CHX oxidations under JSR condition as a function of temperature, with initial pressure of 60bar and Φ of 1.